Rev. LatinAm. Metal. Mat.

Artículo Regular

www.rlmm.org

LATTICE PARAMETER VALUES AND PHASE TRANSITIONS FOR THE Cu_2-II-IV-$S_4(Se_4)$ (II=Mn, Fe, Co; IV=Si, Ge, Sn) MAGNETIC SEMICONDUCTOR COMPOUNDS

Miguel Quintero[1], Ekadink Moreno[1], Silvana Alvarez[1,2], Jesús Marquina[2], Carlos Rincón[2], Eugenio Quintero[2], Pedro Grima[2], José-Antonio Heano[3], Mario Alberto Macías[3]*

1: Centro de Estudios de Semiconductores (CES), Departamento de Física, Facultad de Ciencias, Universidad de los Andes, Mérida 5101, Venezuela. 2: Centro de Estudios Avanzados en Óptica (CEAO), Departamento de Física, Facultad de Ciencias, Universidad de los Andes, Mérida 5101, Venezuela. 3: Grupo de investigación en Química Estructural (GIQUE), Facultad de Ciencias, Escuela de Química, Universidad Industrial de Santander, Apartado aéreo 678, Bucaramanga, Colombia.

** e-mail: mquinter@ula.ve*

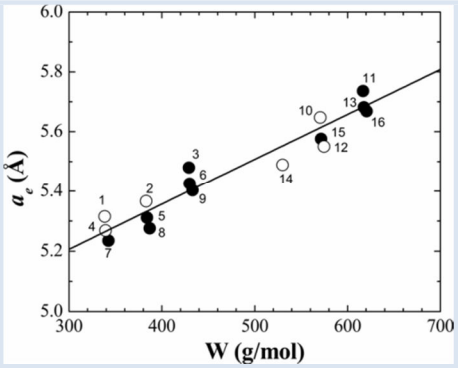

ABSTRACT

X-ray powder diffraction measurements, at 300 K, and differential thermal analysis (DTA) were made on sixteen polycrystalline samples of Cu_2-II-IV-$S_4(Se_4)$ (II: Mn, Fe, Co; IV: Si, Ge, Sn) magnetic semiconductor compounds. The diffraction patterns were analyzed to determine lattice parameter values. The results showed that ten have tetragonal stannite $I\bar{4}2m$ structure, one has tetragonal pseudo-cubic $P\bar{4}$ structure, four an orthorhombic wurtz-stannite $Pmn2_1$ and two an orthorhombic pseudo-cubic F222 structure. When the values of the effective parameter $a_e = (V/N)^{1/3}$ are plotted against its molecular weight W, it was found that the tetragonal and orthorhombic materials lie on the same straight line. The peaks on the DTA measurements were used to determine the type of melting as well as the melting temperature. The resulting data together with the Lindemann relation were used to estimate values for the Debye temperature θ_D as well as for the sound velocity in the material v_s.

Keywords: Semiconducting, X-ray diffraction (XRD), differential thermal analysis (DTA).

VALORES DE LOS PARAMETROS DE LA RED Y TRANSICIONES DE FASE PARA LOS COMPUESTOS SEMICONDUCTORES MAGNETICOS Cu_2-II-IV-S_4(Se4) (II=Mn, Fe, Co; IV=Si, Ge, Sn)

RESUMEN

Se hicieron medidas de difracción en polvo de rayos X (a 300 K) y análisis térmico diferencial (ATD) sobre dieciseis muestras policristalinas de los compuestos semiconductores magnéticos Cu_2-II-IV-$S_4(Se_4)$ (II: Mn, Fe, Co; IV: Si, Ge, Sn). Se analizaron los patrones de difracción para determinar los valores de los parámetros de la red. Los resultados muestran que diez de ellas tiene la estructura *estanita* tetragonal $I\bar{4}2m$, una tiene la estructura tetragonal seudocúbica $P\bar{4}$, cuatro poseen una estructura wurtzita-estannita $Pmn2_1$ y dos tienen una estructura seudocúbica F222. Cuando los valores del parámetro efectivo $a_e = (V/N)^{1/3}$ se grafican contra su peso molecular W, se encuentra que los materiales tetragonales y ortorrómbicos caen sobre la misma línea recta. Los picos en las medidas de ATD fueron usados para determinar el tipo de fusión, así como, la temperatura de fusión. Los datos resultantes junto con la relación de Lindemann fueron utilizados para estimar los valores de la temperatura de Debye θ_D, así como, los valores de la velocidad del sonido en el material v_s.

Palabras Claves: Semiconductores, difracción de rayos X (DRX), análisis térmico diferencial (ATD).

1. INTRODUCTION

Quaternary semiconducting compounds of the I_2-II-IV-VI_4 type, where II = Zn, Cd, Hg, Mn, Fe or Co, IV = Si, Ge, Sn or Pb and VI = S, Se or Te, are of great interest because of both their applications in the fabrication of low cost solar cells [1] and their large magneto-optical effects which are observed when II are paramagnetic atoms [2, 3]. As reported by several authors [3-5], most of these compounds showed either the tetrahedral tetragonal stannite ($I\bar{4}2m$) structure based on zinc-blende, an orthorhombic superstructure derived from wurtzite (known as wurtz-stannite, $Pmn2_1$) or an orthorhombic face-centered unit cell (space group F222) [5]. More recently, it has been found that at room temperature the Cu_2FeSnS_4 compound crystalizes in a tetragonal structure with space group $P\bar{4}$ [6]. The crystallographic parameter values of the I_2-Mn-IV-VI_4, I_2-Fe-IV-VI_4 and of the set Cu_2-II-IV-S_4(Se_4) have been reported in [7, 8, and 4], respectively. The magnetic behavior of various I_2-(Mn,Fe,Co)-IV-VI_4 have been given in [9,10 and 11]. However, the available information related to differential thermal analysis DTA and phase transition temperatures for these compounds is very scarce. The knowledgement of the crystallographic parameters as well as the phase relations of the materials are important to establish their crystal growth conditions. Here, a systematic study on the crystallographic parameters and phase transitions, carried out on Cu_2-(Mn,Fe,Co)-IV-S_4(Se_4) compounds is presented. The obtained crystallographic parameters and melting temperature values together with the Lindemann's relation have been used to estimate values of the Debye temperature as well as the sound velocity in the material.

2. EXPERIMENTAL PART

The samples were produced by the melt and anneal technique. In each case, highly pure components (copper 99.98 %, manganese 99.97 %, iron 99.9 %, cobalt 99.99 %, silicon 99.999%, germanium 99.999%, tin 99.999 %, sulphur 99.997 % and/or selenium 99.9997 %) of 1 g sample were sealed under vacuum (≈ 10^{-5} Torr) in a small quartz ampoule, and then the components were heated up to 200 °C and kept for about 1-2 h, then the temperature was raised to 500 °C using a rate of 40 K/h, and held at this temperature for 14 hour. After, the samples were heated from 500 °C to 800 °C at a rate of 30 K/h and kept at this temperature for another 14 hours. Then it was raised to 1150 °C at 60 K/h, and the components were melted together at this temperature. The furnace temperature was brought slowly (4 K/h) down to 600 °C, and the samples were annealed at this temperature for 1 month. Then, the samples were slowly cooled to room temperature using a rate of about 2 K/h.

A small amount of each compound was gently ground in an agate mortar and sieved to a grain size of less than 38 μm. Each sample was mounted on a zero-background specimen holder for the respective measurement. X-ray powder diffraction patterns of the samples were recorded using a D8 FOCUS BRUKER Rigaku D/MAX IIIB diffractometer operating in Bragg-Brentano geometry equipped with an X-ray tube (Cu Kα radiation: λ = 1.5406 Å, 40 kV and 40 mA) using a nickel filter and an one-dimensional LynxEye detector. A fixed antiscatter slit of 8 mm, receiving slit of 1 mm, soller slits of 2.5 ° and a detector slit of 3 mm were used. The scan range was from 2 to 70 ° 2θ with a step size of 0.02 ° 2θ and a counting time of 0.4 s/step.

Phase transition temperatures were obtained from differential thermal analysis (DTA) measurements, in the temperature range between 20 ºC and 1150 ºC, using a Perkin-Elmer DTA-7 with aluminum and gold used as reference materials. The charge was of powdered alloy of approximately 100-mg weight. Both heating and cooling runs were carried out on each sample, the average rates of these runs being approximately 10 K/min. The error in determining these temperatures is of about ±10 K.

3. RESULTS

3.1 X-Ray

From the X-ray diffraction pattern obtained for each sample, which was indexed with the computer program DICVOL04 [12] using an absolute error of 0.03º (2θ) in the calculations, lattice parameter values were estimated. The space group was established using CHECKCELL program according to the systematic absences, and the unit cell parameters for each compound were refined with the NBS*AIDS83 program [13]. A complete crystal structure refinement was performed for each compound using the fitting program MAUD (Material Analysis Using Diffraction) [14]. The obtained crystallographic parameter values and

space groups are summarized in table 1.

It is seen from table 1 that, as indicated above, the present materials crystallize in two tetragonal ($I\bar{4}2m$, $P\bar{4}$) and two orthorhombic ($Pmn2_1$, F222) tetrahedral structure types. Out of the 16 slowly cooled samples investigated in this work, ten were found to be tetragonal stannite $I\bar{4}2m$, one was tetragonal pseudo-cubic $P\bar{4}$, four were orthorhombic wurtz-stannite $Pmn2_1$ and two were orthorhombic pseudo-cubic F222. The x-ray diffraction patterns obtained here are similar to those shown in Ref. (15) for stannite $I\bar{4}2m$ and wurtz-stannite $Pmn2_1$, Ref. 6 for tetragonal $P\bar{4}$ and Ref. (5) for orthorhombic F222.

Table 1. Resulting lattice parameter, melting point (T_M), Debye temperature (θ_D) and sound velocity (v_S) values for each compound. N is the number of molecules per cell, SG the space group.

N°	Compound	W (g/mol)	N	SG	a (Å)	b (Å)	c (Å)	V (Å^3)	a_e (Å)	D_x (g/cm^3)	T_M (K)	θ_D (K)	$v_s \times 10^5$ (cm/s)
1	Cu_2MnSiS_4	338.38	2	$Pmn2_1$	7.5362	6.4416	6.1866	300.33	5.3152	3.74	1293	312	2.8
2	Cu_2MnGeS_4	382.93	2	$Pmn2_1$	7.6160	6.5130	6.2300	309.03	5.3661	4.12	1272	288	2.6
3	Cu_2MnSnS_4	429.00	2	$I\bar{4}2m$	5.5180	5.5180	10.8070	329.06	5.4796	4.33	1177	257	2.4
4	Cu_2FeSiS_4	339.28	2	$Pmn2_1$	7.4210	6.4170	6.1409	292.43	5.2682	3.85	1275	311	2.7
5	Cu_2FeGeS_4	383.84	2	$I\bar{4}2m$	5.3355	5.3355	10.5250	299.62	5.3111	4.25	1269	289	2.6
6	Cu_2FeSnS_4	429.91	1	P-4	5.4329	5.4329	5.4104	159.70	5.4254	4.47	1104	250	2.3
7	Cu_2CoSiS_4	342.37	2	$I\bar{4}2m$	5.2683	5.2683	10.3350	286.85	5.2345	3.96	1258	312	2.7
8	Cu_2CoGeS_4	479.59	2	$I\bar{4}2m$	5.2957	5.2957	10.4740	293.74	5.2761	4.37	1323	299	2.6
9	Cu_2CoSnS_4	433.00	2	$I\bar{4}2m$	5.3992	5.3992	10.8180	315.36	5.4025	4.56	1191	261	2.4
10	$Cu_2MnGeSe_4$	570.51	2	$Pmn2_1$	7.9958	6.8574	6.5717	360.33	5.6479	5.26	1085	207	2.0
11	$Cu_2MnSnSe_4$	616.58	2	$I\bar{4}2m$	5.7623	5.7623	11.3682	377.47	5.7361	5.42	967	185	1.8
12	$Cu_2FeGeSe_4$	571.42	2	$I\bar{4}2m$	5.6008	5.6008	11.0561	346.82	5.5764	5.47	1046	206	1.9
13	$Cu_2FeSnSe_4$	617.49	2	$I\bar{4}2m$	5.7054	5.7054	11.2710	366.89	5.6820	5.59	1045	194	1.9
14	$Cu_2CoSiSe_4$	529.95	1	F222	5.5680	5.5010	5.3980	165.34	5.4886	5.32	1112	224	2.1
15	$Cu_2CoGeSe_4$	574.51	1	F222	5.5983	5.5548	5.4993	171.01	5.5507	5.58	1054	207	1.9
16	$Cu_2CoSnSe_4$	620.58	2	$I\bar{4}2m$	5.6728	5.6728	11.3220	364.35	5.6689	5.66	1118	201	1.9
a	$Cu_2CdGeSe_4$	627.98	2	$I\bar{4}2m$	5.7482	5.7482	11.0533	365.22	5.6734	5.71	1103	198	1.9
b	$Cu_2CdSnSe_4$	674.05	2	$I\bar{4}2m$	5.8306	5.8306	11.399	387.52	5.7867	5.78	1040	182	1.8
c	Cu_2CdGeS_4	440.40	2	$Pmn2_1$	7.703	6.5549	6.312	318.71	5.4215	4.59	1282	267	2.4
d	$Cu_2HgSnSe_4$	762.23	2	$I\bar{4}2m$	5.818	5.818	11.48	388.59	5.7919	6.51	981	166	1.6
e	$Cu_2ZnSnSe_4$	627.03	2	$I\bar{4}2m$	5.681	5.681	11.34	365.98	5.6773	5.69	1063	195	1.9

a: Ref. [17]; b: Ref. [16]; c: Ref. [26]; d: Ref. [25]; e: Ref. [25].

3.2 Differential Thermal Analysis DTA

DTA runs were carried out on each prepared sample as indicated above. The transition temperatures as well as the type of melting were obtained from the peaks on the DTA heating and cooling curves. Each transition temperature was determined from the base intercept of the tangent to the leading edge of the peak in the differential signal. Values of the melting point temperature, denoted as T_M, obtained from the congruent and/or peritectic peaks on the DTA curves are given in table 1. The DTA results for the investigated samples can be summarized as follow. The DTA curves for the Cu_2FeSnS_4 [6], $Cu_2MnGeSe_4$ [15], $Cu_2FeGeSe_4$ [15], $Cu_2MnSnSe_4$ [16] and $Cu_2FeSnSe_4$ [16] have been given in earlier works. The resulting transition temperature values, melting type and phase relations have been collected in table 2.

Table 2. Values of transition temperatures obtained from heating T_H and cooling T_C DTA runs.

No	*Compound*	T_H (°C)	T_C (°C)	*Melting Type*	*Phase relations*	*Ref.*
1	Cu_2MnSiS_4	1020	1146, 1002, 986	Peritectic	$\delta \rightarrow \beta + \delta \rightarrow \beta \rightarrow L + \beta_1 \rightarrow L$	PW
2	Cu_2MnGeS_4	999, 1029	986	Undercooling Peritectic	$\delta \rightarrow L + \delta_1 \rightarrow L$	PW
3	Cu_2MnSnS_4	904	1004, 903	Peritectic	$\alpha \rightarrow L + \delta_1 \rightarrow L$	PW
4	Cu_2FeSiS_4	1002, 919	996, 920	Congruent	$\delta \rightarrow \alpha \rightarrow L$	PW
5	Cu_2FeGeS_4	996,1024	960	Undercooling Peritectic	$\alpha \rightarrow L + \delta_1 \rightarrow L$	PW
6	Cu_2FeSnS_4	831	831	Congruent	$\gamma \rightarrow \alpha \rightarrow L$	[6]
7	Cu_2CoSiS_4	985, 923	1047, 985, 870	Peritectic	$\alpha \rightarrow \alpha + \delta \rightarrow \delta \rightarrow L + \delta_1 \rightarrow L$	PW
8	Cu_2CoGeS_4	1050	1014	Undercooling Undetermined	$\alpha \rightarrow L$	PW
9	Cu_2CoSnS_4	918	918, 871	Congruent	$\alpha \rightarrow \delta \rightarrow L$	PW
10	$Cu_2MnGeSe_4$	812, 688	848	Peritectic	$\delta \rightarrow L + \delta_1 \rightarrow L$	[15]
11	$Cu_2MnSnSe_4$	694, 795, 613	700, 606	Undercooling Peritectic	$\alpha \rightarrow \alpha + \delta \rightarrow L + \delta_1 \rightarrow L$	[16]
12	$Cu_2FeGeSe_4$	773	734	Undercooling Undetermined	$\alpha \rightarrow L$	[15]
13	$Cu_2FeSnSe_4$	772	740	Undercooling Peritectic	$\alpha \rightarrow \alpha + \delta \rightarrow L + \delta_1 \rightarrow L$	[16]
14	$Cu_2CoSiSe_4$	839, 908, 711	907, 822	Peritectic	$\delta \rightarrow \delta + \beta \rightarrow \beta \rightarrow L + \beta_1 \rightarrow L$	PW
15	$Cu_2CoGeSe_4$	781, 866	811, 746	Undercooling Peritectic	$\gamma' \rightarrow L + \beta \rightarrow L$	PW
16	$Cu_2CoSnSe_4$	845, 895, 675	854, 674	Peritectic	$\alpha \rightarrow \beta \rightarrow L + \beta_1 \rightarrow L$	PW

PW: Present work. α: tetragonal stannite $I\bar{4}2m$ structure; δ: orthorhombic wurtz-stannite $Pmn2_1$ structure; δ_1: high temperature modification HT; γ: tetragonal pseudo-cubic $P\bar{4}$; γ': orthorhombic pseudo-cubic F222 structure; β and β_1-HT: cubic zinc-blende.

3.2.1 Cu_2MnSiS_4, Cu_2MnGeS_4 and Cu_2MnSnS_4.

From the obtained DTA thermograms for Cu_2MnSiS_4, shown in fig. 1, it is seen that only one transition at about 1020 ºC appears in the heating curve, while the cooling run shows three transitions at 1146 and 1002 and 986 ºC. The effects observed at 1020 and 1146 ºC would correspond to the solid and liquid lines respectively, i.e. to the peritectic decomposition of the Cu_2MnSiS_4 (from β to liquid L+ β_1) and to the transition to the liquid L state (from L+ β_1 to L), respectively. Here, β_1 and β must be cubic zinc-blende phases with different compositions since, at low temperatures, the tetragonal stannite α phase ($I\bar{4}2m$) has lower symmetry than the wurtz-stannite δ phase ($Pmn2_1$) observed in the x-ray results given above. In the range between 1020 and 1002 ºC the phase is β, below 1002 ºC there is a two phase field β + δ, and at 986 ºC a solid-solid transition from β + δ to δ occurs, where once again δ has the wurtz-stannite structure shown by the present x-ray data . These results are similar to those reported in earlier works for the compounds $Cu_2CdGeSe_4$ [15, 17] and $Cu_2ZnGeSe_4$ [18, 19]. From the DTA results for Cu_2MnGeS_4 shown in fig. 2, it can be observed that the respective DTA curves exhibit two effects in both heating and cooling runs. Also, the onset temperature in the heating processes (999 ºC) is slightly higher than the one in the cooling run (986 ºC). This behavior would indicate that undercooling effects are present. The DTA results show that the Cu_2MnGeS_4 melts incongruently and the peritectic decomposition (from δ to L+δ_1) occurs at 999 ºC and the liquid transformation (from L+δ_1 to L) takes place at 1029 ºC. The DTA thermograms for the Cu_2MnSnS_4 are shown in fig. 3, which are similar to the ones in fig. 1. It is seen from this figure that one transition at about 904 ºC occurs in the heating curve, while the cooling run shows two transitions at 1004 and 904 ºC. The effects observed at around 904 ºC in both of these two runs and at 1004 ºC in the cooling one would correspond to the peritectic decomposition of the Cu_2MnSnS_4 (from α to liquid L+δ_1) and to the liquid transformation (from L+ δ_1 to L), respectively, where δ_1 being the HT modification suggested in earlier works for similar compounds [15, 17, 18, 19] and α the tetragonal stannite observed in the present x-ray diffractogram, respectively.

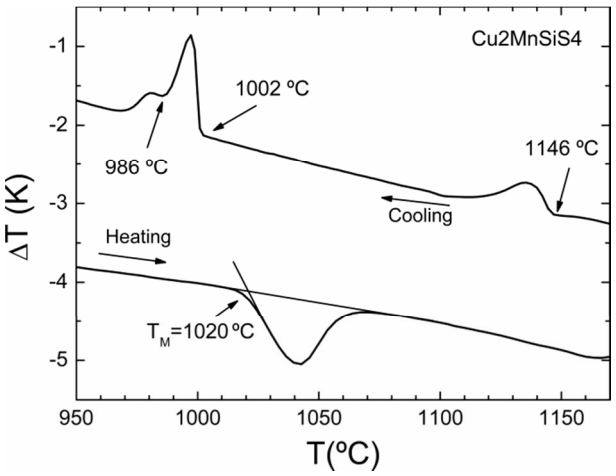

Figure 1. DTA thermograms for Cu_2MnSiS_4. The direction of heating run, or cooling run, is indicated by the corresponding arrow.

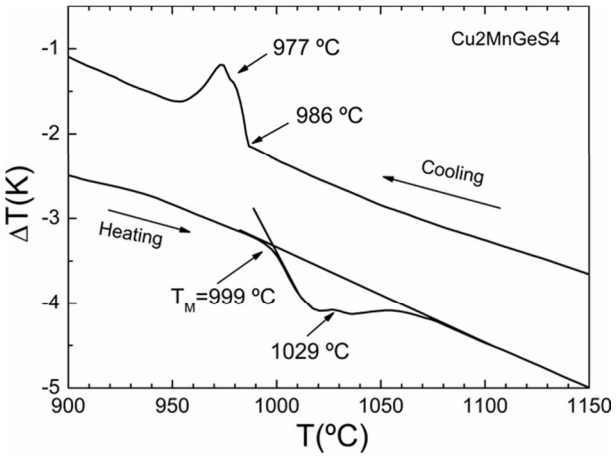

Figure 2. DTA thermograms for Cu_2MnGeS_4. The direction of heating run, or cooling run, is indicated by the corresponding arrow.

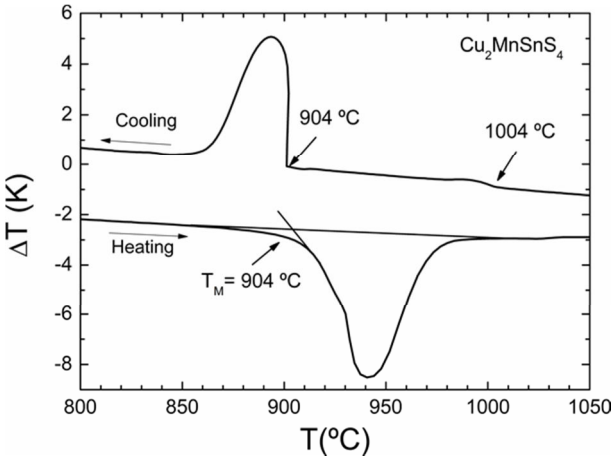

Figure 3. DTA thermograms for Cu_2MnSnS_4. The direction of heating run, or cooling run, is indicated by the corresponding arrow.

3.2.2 Cu_2FeSiS_4 and Cu_2FeGeS_4.

From the DTA thermograms for Cu_2FeSiS_4 shown in fig. 4, it is seen that the DTA curves exhibit two effects in both heating (at 919 and 1002 ºC) and cooling (at 996 and 920 ºC) runs. In addition, no effects due to undercooling are observed, and the compound melts congruently at about 1002 ºC. The DTA results for Cu_2FeGeS_4 (see fig. 5) show that the compound melts incongruently and undercooling behavior is present. Thus, the peritectic decomposition (from α to L+δ_1) occurs at 996 ºC and the liquid (from δ_1+L to L) at 1024 ºC, where δ_1 is the HT modification suggested in earlier works [15, 17, 18, 19] and α the tetragonal stannite ($I\bar{4}2m$) observed in the present x-ray results.

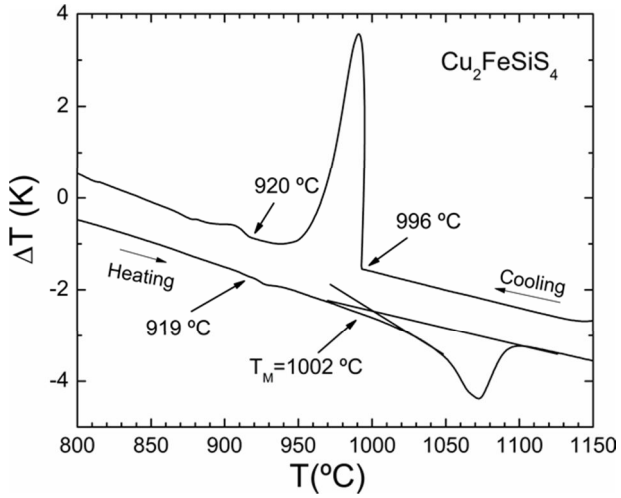

Figure 4. DTA thermograms for Cu_2FeSiS_4. The direction of heating run, or cooling run, is indicated by the corresponding arrow.

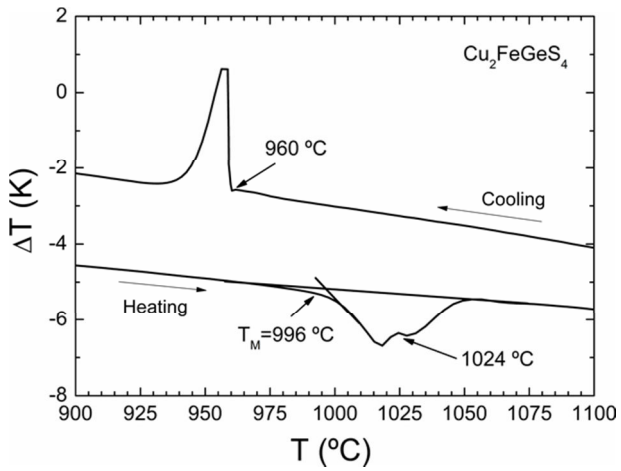

Figure 5. DTA thermograms for Cu_2FeGeS_4. The direction of heating run, or cooling run, is indicated by the corresponding arrow.

3.2.3 Cu_2CoSiS_4, Cu_2CoGeS_4 and Cu_2CoSnS_4.

The resulting DTA thermograms for Cu_2CoSiS_4 are illustrated in fig. 6. It is seen that the DTA curves exhibit two effects in the heating run at 923 and 1041 ºC, while the cooling run shows three transitions at 1047, 985 and 870 ºC. No effects due to undercooling are observed in this compound. The effects observed at 985 and 1041 ºC would correspond to the peritectic decomposition of the Cu_2CoSiS_4 (from δ to liquid L+δ_1) and to the liquid L state (from L+δ_1 to L), respectively. In the range between 985 and 923 ºC, the phase is δ and at 870ºC a transition occurs from δ+α to the tetragonal stannite α phase ($I\bar{4}2m$), which is the equilibrium structure at 300 K. From the DTA curves for Cu_2CoGeS_4 (see fig. 7) it is observed that the onset temperature in the heating process (1050 °C) is slightly higher than the one in the cooling run (1014 °C). This would indicate that undercooling effects are present so that the type of melting is uncertain in this case. The melting point of this compound is estimated to be $T_M \approx 1050$ ºC, from the heating process. The obtained DTA results for Cu_2CoSnS_4, shown in fig. 8, indicate that the compound melts congruently at 918 ºC whereas below 871 ºC the phase is the tetragonal stannite α ($I\bar{4}2m$), which is the equilibrium structure at 300 K.

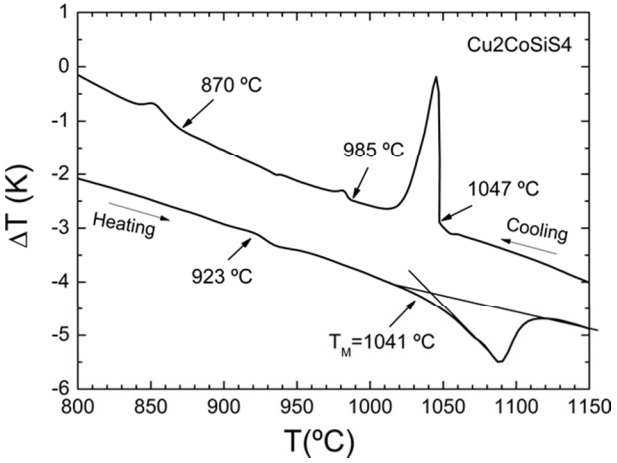

Figure 6. DTA thermograms for Cu_2CoSiS_4. The direction of heating run, or cooling run, is indicated by the corresponding arrow.

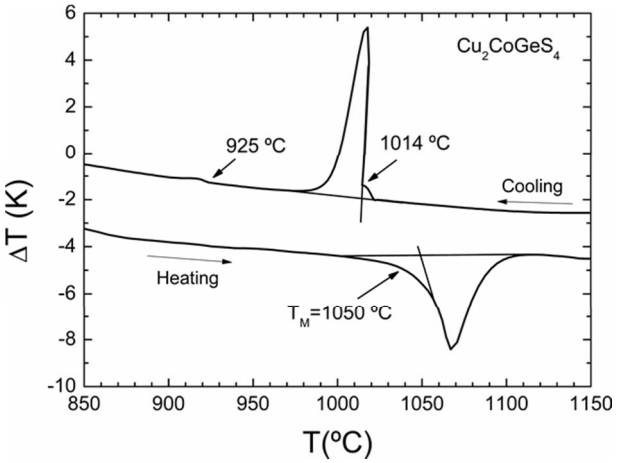

Figure 7. DTA thermograms for Cu_2CoGeS_4. The direction of heating run, or cooling run, is indicated by the corresponding arrow.

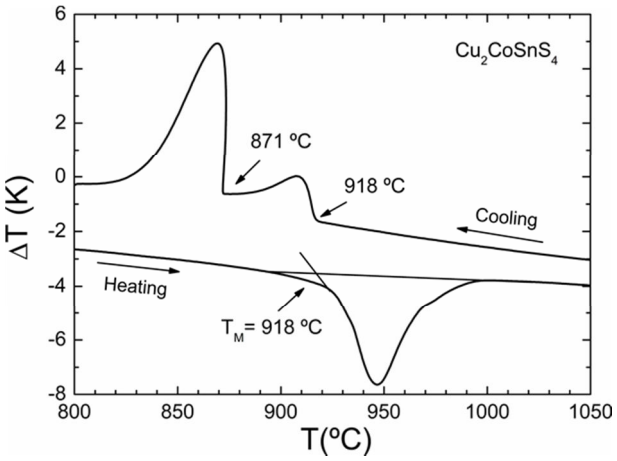

Figure 8. DTA thermograms for Cu_2CoSnS_4. The direction of heating run, or cooling run, is indicated by the corresponding arrow.

3.2.4 $Cu_2CoSiSe_4$, $Cu_2CoGeSe_4$ and $Cu_2CoSnSe_4$.

From the DTA curves for $Cu_2CoSiSe_4$, shown in fig. 9, three transitions occurring at about 711, 839 and 908 ºC and two transformations at 907 and 822 ºC can be observed in the heating and cooling runs, respectively. Undercooling effects are not observed in the present case. The peaks at 839 and 908 ºC in the heating curve are related to the peritectic decomposition of the compound (from β to L+β_1) and to the liquid transformation (from L+β_1 to L), respectively. Once again, β_1 and β are cubic zinc blende phases of different compositions. A two phase field β+δ exits below 822 ºC and a transformation from β+δ to the wurtz-stannite δ phase ($Pmn2_1$) observed in the x-ray data occurs at 711 ºC. From the DTA results for the $Cu_2CoGeSe_4$, fig. 10, it was found that undercooling effects are present. Also, it is seen that this compound melts incongruently at 781 ºC and below this temperature the structure is γ orthorhombic pseudocubic (F222). The DTA thermograms for the $Cu_2CoSnSe_4$ are shown in fig. 11; it can be observed in this figure that it has a peritectic temperature of $T_M \approx 845$ ºC (β → L + β_1) and the liquid (L + β_1 → L) occurs at 895 ºC. Below 675 ºC, the phase is the tetragonal stannite α ($I\bar{4}2m$), which is the equilibrium structure at room temperature.

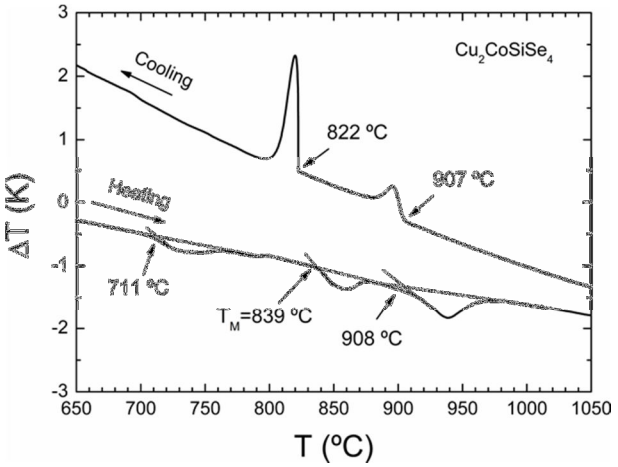

Figure 9. DTA thermograms for $Cu_2CoSiSe_4$. The direction of heating run, or cooling run, is indicated by the corresponding arrow.

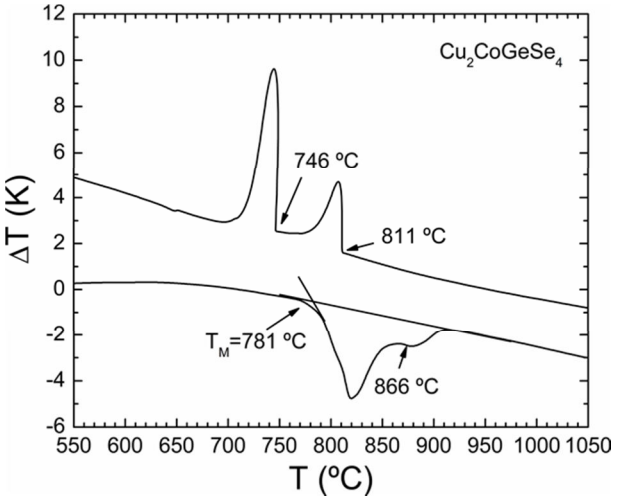

Figure 10. DTA thermograms for $Cu_2CoGeSe_4$. The direction of heating run, or cooling run, is indicated by the corresponding arrow.

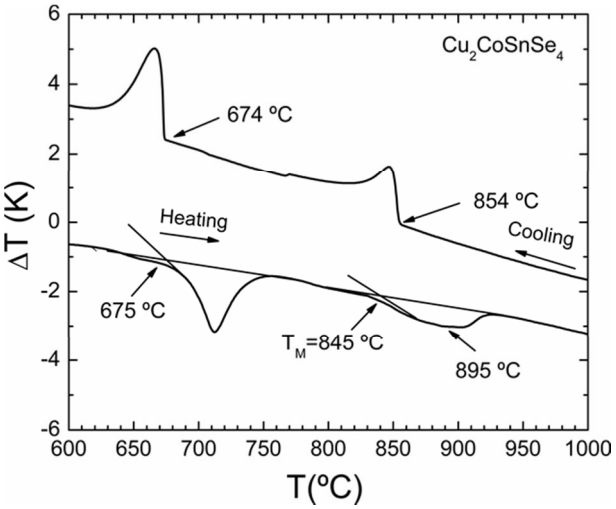

Figure 11. DTA thermograms for $Cu_2CoSnSe_4$. The direction of heating run, or cooling run, is indicated by the corresponding arrow.

4. DISCUSSION

As has been shown previously [9] for these type of compounds, the quantity $a_e = (V/N)^{1/3}$, where V is the volume of the unit cell and N the number of molecules per cell, varied smoothly with the molecular weight W of the compound. For the present materials, N depends upon the corresponding space group, thus N = 2 for $I\bar{4}2m$ or $Pmn2_1$ and N = 1 for $P\bar{4}$ or F222. Values of a_e for the compounds investigated here are given in table 1. Figure 12 shows the variation of a_e vs W for the tetragonal and orthorhombic. It is seen from this figure that, within the limits of experimental errors, for the present Cu_2(Mn,Fe,Co)-IV-S_4(Se_4), whether tetragonal or orthorhombic phases, the experimental points of a_e lie on the same straight line. It is to be mentioned that, in a previous work, carried out on material involving Fe atoms [8], all of the compounds with Ag and Te atoms were found to be orthorhombic, and their a_e values lied on a straight line different than the one for the tetragonal compounds. However, in the work made on the I_2-Mn-IV-VI_4 [7], the results showed that the tetragonal as well as the orthorhombic Cu-compounds lie on the same straight line, while the Ag materials lie on a different one. The present results are in good agreement with the ones obtained for the Cu compounds in Ref. [7].

Another point of interest here is to use the obtained values of a_e and the melting temperature T_M to estimate values for the Debye temperature θ_D with the Lindemann's expresion [20].

$$\theta_D = C\left(\frac{T_{HM}}{\overline{W}}\right)^{1/2}\left(\frac{1}{a_e}\right) \qquad (1)$$

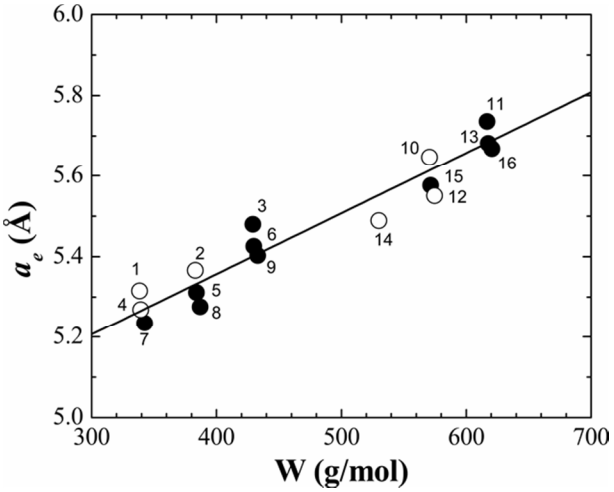

Figure 12. Variation of effective lattice parameter a_e with molecular weight W for I_2-Mn,Fe,Co-IV-VI_4. Full circles: tetragonal. Open circles: orthorhombic. The solid line is to guide the eyes.

Where $\overline{W} = W/n$, n is the number of atoms per formula (n = 8 for the present quaternaries), V is the volume of unit cell (in $Å^3$) and C is a constant. The Debye temperature is an important parameter in the understanding of thermal and electrical properties of semiconducting materials. A value of C = 450 has been used for NaCl structure type [21] and Garbato et al [22] have used C =341 for the tetrahedral bonded tetragonal chalcopyrite as well as hexagonal wurtzite materials. A value of C is not available for the I_2-II-IV-VI_4 tetrahedral bonded quaternary compounds as yet. Also, no directly experimental values of θ_D for the present compounds have been given in the literature. Since the ternary chalcopyrite structure of the I-III-VI_2 materials is close to the tetragonal one of most of the present tetrahedral bonded quaternary compounds, available θ_D experimental data for ternary compounds can be used for an estimation of C. Thus, the values of θ_D determined from specific heat experiments for the I-III-VI_2 [23, 24] have been plotted as a function of $W^{-1/2}$ in fig. 13. Using these values together with the T_M [22-24, 27-32] and W values in eq. (1), a value of C ≈ 300 is obtained from the average of the C values for the I-III-VI_2 compounds. Hence, as first approximation, here the values of a_e and T_M listed respectively in table I have been used in Eq. (1),

with C ≈ 300, to estimate initial values of θ_D for the present Cu_2-(Mn,Fe,Co)-IV-S_4(Se_4) compounds. The resulting θ_D values for the I2-II-IV-VI_4, quaternaries together with the experimental ones for the I-III-VI_2 are shown in fig. 13. In addition, values θ_D for some nonmagnetic I_2-II-IV-VI_4, for which experimental values of a_e and T_M are available, have also been included in this figure. The estimated values of θ_D for the materials are tabulated in table I. It seen from this fig. 13 that, within the limits of experimental errors, these curves of θ_D vs $W^{-1/2}$ are linear, and the values for the quaternaries are higher than the ones for the ternaries. Since the T_M and W values for ternary and quaternary compounds are very similar, then the separation between both θ_D vs $W^{-1/2}$ is due to that the values of ae for the quaternaries are greater than the ones for the ternaries.

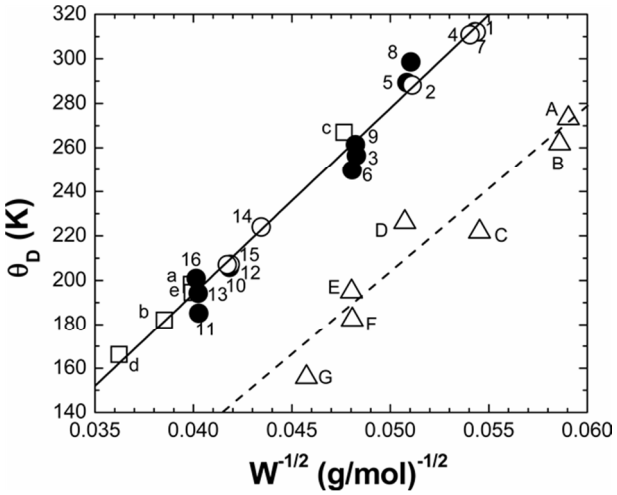

Figure 13. Variation of the Debye temperature θ_D vs $(W)^{-1/2}$. Close circles: tetragonal. Open circles: orthorhombic. The triangles represent the experimental θ_D values from specific heat for the I-III-VI_2 compounds. A. $CuInS_2$ [24], B. $CuInSe_2$ [24], C. $CuGaSe_2$ [24], D. $CuInTe_2$ [24], E. $CuGaTe_2$ [24], F.$AgInTe_2$ [23], G.$AgGaTe_2$ [23]. The squares represent some non-magnetic I_2-II-IV-VI_4: a. $Cu_2CdGeSe_4$ [17], b. $Cu_2CdSnSe_4$ [16], c. Cu_2CdGeS_4 [26], d. $Cu_2HgSnSe_4$ [25], e. $Cu_2ZnSnSe_4$ [25]. The solid line represents the fit to a linear form in $W^{-1/2}$. The dashed line is to guide the eyes.

The sound velocity v_s in a material can be estimated from the value of the Debye temperature θ_D by the well-known relation [33],

$$v_s = \frac{k_B \theta_D}{\hbar}\left(\frac{\bar{V}}{6\pi^2}\right)^{1/3} \qquad (2)$$

where k_B is the Boltzmann constant, $\hbar$ is the reduced Planck's constant, $\bar{V}$ (= V/16) is the mean volume per atom. The resulting curve of v_s vs $W^{-1/2}$, obtained using the values of V and θ_D from table I with eq. (2), is shown in fig. 14. It is seen from figs. 13 and 14 that, within the limits of the experimental errors, the values of θ_D and v_s vary linearly with $W^{-1/2}$. Hence, as a first approximation, using the molecular weight W of the compound reasonable values of θ_D and/or v_s can be obtained from figs. 13 and 14, respectively, for similar materials. Then for extrapolation purposes, the values of θ_D and vs as a function of $W^{-1/2}$ were least squared fitted to a linear form and the resulting relations are,

$$\theta_D = -141.8 + 8392.0\ W^{-1/2} \quad (K) \qquad (3)$$

$$v_s = -75849.8 + 6.5 \times 106\ W^{-1/2} \quad (cm/s) \qquad (4)$$

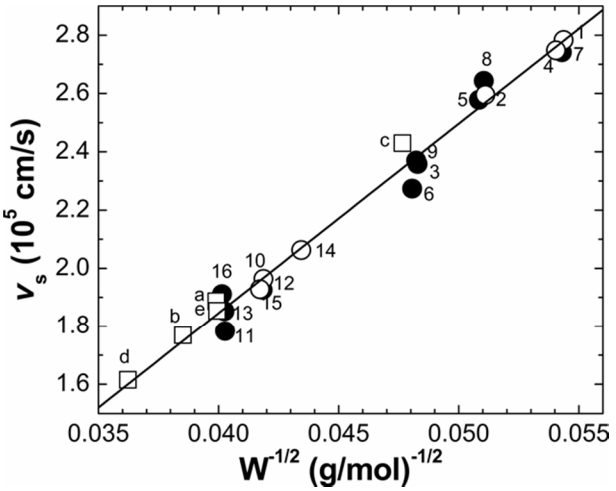

Figure 14. Variation of sound velocity v_s vs $(W)^{-1/2}$. Close circles: tetragonal. Open circles: orthorhombic. The solid line represents the fit to a linear form in $W^{-1/2}$.

5. CONCLUSIONS

The x-ray results show that the present materials crystallize in two tetragonal ($I\bar{4}2m$, $P\bar{4}$) and two orthorhombic ($Pmn2_1$, F222) tetrahedral structure types. When the values of the parameter a_e (= $(V/N)^{1/3}$) are plotted against values of the molecular weight W of the material, it is found that independent of the crystal structure all the

compounds lie on the same straight line in agreement with earlier works made on compounds involving Cu, S and Se but neither Ag, Fe and Te. From the DTA data, it was found that Cu_2FeSiS_4, Cu_2FeSnS_4 and Cu_2CoSnS_4 melt congruently, for Cu_2CoSnS_4, $Cu_2FeSnSe_4$ the melting type could not be determined because undercooling effects are present. The rest of the materials were found to have peritectic melting type. Also, all of the materials were found to have polymorphous transformations. The Lidenmann relation, with C= 300, was found to be appropriated to estimate reasonable values of the Debye temperature θ_D and/or the sound velocity v_s. These values were found to vary linearly with W of the compound, so that a value of θ_D and/or vs for a material can be obtained from W.

6. ACKNOWLEDGEMENTS

This work was partially supported by the CDCHT-ULA (Project No. C-1740-11-05-AA). E. Moreno would like to thank the Plan de Desarrollo de Talentos Humanos de Alto Nivel of FONACIT, through contract No. 200601411, Venezuela. M.A. Macías would like to thank COLCIENCIAS (Colombia) for his doctoral fellowship.

7. REFERENCIAS

[1]. Katagiri H, Jimbo K, Maw WS, Oishi K, Yamazaki M, Araki H, Takeuchi A. Thin Solid Films 2009; 517: 2455-2460.

[2]. Shapira Y, McNiff EJ, Oliveira NF, Honig ED, Dwight K, Wold A. Phys. Rev. B 1988; 37: 411-418.

[3]. McCabe GH, Fries T, Liu MT, Shapira Y, Ram-Mohan LR, Kershaw R, Wold A, Fau C, Averous M, McNiff EJ. Phys. Rev. B 1997; 56: 6673-6680.

[4]. Shafer W, Nitsche R. Mater. Res. Bull. 1974; 9: 645-654.

[5]. Gulay LD, Nazarchuk OP, Olekseyuk ID. J. Alloy Compd. 2004; 377: 306-311.

[6]. Rincón C, Quintero M, Moreno E, Power Ch, Quintero E, Henao JA, Macías MA, Delgado GE, Tovar R, Morocoima M. Solid State Commun. 2011; 151: 947-951.

[7]. Lamarche A-M, Willsher A, Chen L, Lamarche G, Woolley JC. J. Solid State Chem. 1991; 94: 313-318.

[8]. Quintero M, Barreto A, Grima P,Tovar R, Quintero E, Sanchez Porras G, Ruiz J, Woolley JC, Lamarche G and Lamarche A-M. Mater. Res. Bull. 1999; 34: 2263-2270.

[9]. Guen L, Glaunsinger WS. J. Solid State Chem. 1980; 35: 10-21.

[10]. Chen XL, Lamarche A-M, Lamarche G, Woolley JC. J. Magn. Magn. Mater. 1993; 118: 119-128.

[11]. Quintero E, Quintero M, Moreno E, Lara L, Morocoima M, Pineda F, Grima P, Tovar R, Bocaranda P, Henao JA, Macías MA. J. Phys. Chem. Solids 2010; 71: 993-998.

[12]. Boultif A, Louër D. J. Appl. Cryst. 1991; 24: 987-993.

[13]. Laugier J, Bochu B. "Chekcell: Graphical powder indexing cell and space group assignment software" [On-Line], http://www.ccp14.ac.uk/tutorial/lmgp/. Miguel AD, Hubberd CR, Stalick JK. "NBS*AIDS80: A FORTRAN program for crystallographic data evaluation", National Bureau of Standards (USA), Tech. Note 1141.

[14]. Lutterotti L. "Material Analysis using Diffraction-MAUD: Computer code JAVA." Trento: Universite of Trento. 1997-2009 [On-Line], http://www.ing.unitn.it/~maud/.

[15]. Quintero E, Tovar R, Quintero M, Delgado GE, Morocoima M, Caldera D, Ruiz J, Mora AE, Briceño M, Fernadez JL. J. Alloy Compd. 2007; 432: 142-148.

[16]. Moreno E, Quintero M, Morocoima M, Quintero E, Grima P, Tovar R, Bocaranda P, Delgado GE, Contreras JE, Mora AE, Briceño JM, Ávila Godoy R, Fernández JL, Henao JA, Macías MA. J. Alloy Compd. 2009; 486: 212-218.

[17]. Gulay LD, Romanyuk Ya. E, Parasyuk OV. J. Alloy Compd. 2002; 347: 193-197.

[18]. Parasyuk OV, Gulay LD, Romanyuk Ya. E, Piskach LV. J. Alloy Compd. 2001; 329: 202-207.

[19]. Caldera D, Quintero M, Morocoima M, Quintero E, Grima P, Marchan N, Moreno E, Bocaranda P, Delgado GE, Mora AE. J. Alloy Compd. 2008; 457: 221-224.

[20]. Lindemann F. Z. Phys. 1910; 11: 609.

[21]. Neelakanda Pillai N, Mahadevan CK. Physica B 2008; 403: 2168-2172.

[22]. Garbato L, Ledda F, Manca P, Rucci A, Spiga A, "Phase diagram, growth and properties of quaternary diamond-like alloys in the $CuInSe_4$-CdSe System". Mérida (Venezuela) Prog. Cryst. Growth. Ch. 10, 1984 p. 199.

[23]. Bachmann KJ, Hsu FS, Thiel FA, Kasper HM. J. Electron. Mater. 1977; 6: 431-448.

[24]. Bonmhammel K, Deus P, Kühn, Möller. Phys. Status. Solidi (a) 2002; 71: 505-510.

[25]. Olekseyuk ID, Gulay LD, Dydchak IV, Pichach

LV, Parayuk OV, Marchuk OV. J. Alloy Compd. 2002; 340: 141-145.

[26]. Pisckach LV, Parasyuk OV, Romanyuk Ya. E. J. Alloy Compd. 2000; 299: 227-231.

[27]. Komaki H, Yoshino K, Seto S, Yoneta M, Akaki Y, Ikary T. J. Cryst. Growth 2002; 236: 253-256.

[28]. Meriono JM, Di Michiel M, León M. J. Phys. Chem. Solids 2003; 64: 1649-1652.

[29]. Burger A, Ndap JO, Cui Y, Roy U, Morgan S, Chattopadhyay K, Ma X, Faris K, Thibaud S, Miles R, Mateen H, Goldstein JT, Rawn CJ. J. Cryst. Growth 2001; 225: 505-511.

[30]. Roy UN, Mekonen B, Adetunji OO, Chattopadhyay K, Kochari F, Cui Y, Burger A, Goldstein JT. J. Cryst. Growth 2002; 241: 135-140.

[31]. Klimova AM, Ananichev VA, Blinov LN. Glass Phys. Chem+ 2006; 32:643.

[32]. Jagomägi A, Krustok J, Raudoja J, Grossberg M, Danilson M, Yakushev M. Physica B 2003; 337: 369-374.

[33]. G. Sánchez Porras, M. Quintero and S.M. Wasim. J. Applied Physics 1990, 67 (7), 3382-3386.